ACADEMIC PRESS

Available online at www.sciencedirect.com
SCIENCE DIRECT®

Journal of Colloid and Interface Science 257 (2003) 93–107

JOURNAL OF
Colloid and
Interface Science

www.elsevier.com/locate/jcis

Film drainage between two surfactant-coated drops colliding at constant approach velocity

Leslie Y. Yeo, Omar K. Matar,* E. Susana Perez de Ortiz, and Geoffrey F. Hewitt

Department of Chemical Engineering and Chemical Technology, Imperial College of Science, Technology and Medicine, Prince Consort Road, London SW7 2BY, UK

Received 13 August 2001; accepted 17 September 2002

Abstract

The drainage of the intervening continuous phase film between two drops approaching each other at constant velocity under the influence of insoluble surfactant is investigated. The mathematical model to be solved is a coupled pair of fourth-order nonlinear partial differential equations which arise from the relationships governing the evolution of the film thickness and the surfactant interfacial concentration in the lubrication approximation. We adopt a simplified approach which uses lubrication theory to describe the flow within the drop, marking a departure from the conventional framework in which Stokes flow is assumed. When the model is solved numerically together with the relevant initial and boundary conditions, the results obtained are compared with those found in the literature using the "boundary integral" method to solve for the flow in the drop phase. The close agreement between the results inspires confidence in the predictions of the simplified approach adopted. The analysis on the effect of insoluble surfactant indicates that its presence retards the drainage of the film: The fully immobile interface limit is recovered even in the presence of a small amount of surfactant above a critical concentration; film rupture is either prolonged or prevented. The retardation of the film was attributed to gradients of interfacial tension which gave rise to the Marangoni effect. A study of the influence of various system parameters on the drainage dynamics was conducted and three regimes of drainage and possible rupture were identified depending on the relative magnitudes of the drop approach velocity and the van der Waals interaction force: Nose rupture, rim rupture, and film immobilization and flattening. Finally, the possibility of forming secondary droplets by encapsulating the continuous phase film into the coalesced drop at rupture was examined and quantified in light of these regimes.

Keywords: Drop coalescence; Insoluble surfactant; Film drainage; Film rupture; Marangoni effect; Emulsions; Secondary dispersions

1. Introduction

Understanding the coalescence phenomenon between two drops plays a crucial role in determining the stability of liquid–liquid processes. The coalescence process occurs as the drops approach each other and, as a result, trap a thin film of the continuous phase between the drop interfaces. Under the influence of the interaction forces that act on the drop, the drop interfaces begin to deform slightly and the intervening continuous phase film proceeds to drain. At a thickness of approximately 1000 Å [1], intermolecular forces such as the van der Waals force (and for much thinner films, electric double-layer forces) become significant and dominate the final stages of the film drainage process. In cases wherein the van der Waals force overcomes the restoring electric double-layer force, there is a resultant negative contribution to the disjoining pressure, resulting in the destabilization of the film leading to rupture.

For pure systems in which surface-active materials are not present, studies to investigate the film drainage hydrodynamics were conducted for bubbles or drops approaching a horizontal interface [2–4]. Subsequent work extending the analysis to include systems of colliding bubbles or drops have been presented by Chen [1], Li [5], Klaseboer et al. [6] and others. In reality, surfactants, whether present in minute quantities as trace impurities or intentionally added to the dispersion in the form of additives, are often present in liquid–liquid systems. In such cases, the interfacial properties of the system are often altered by the surfactant, resulting in interfacial tension gradients which, in turn, give rise to additional tangential stresses at the interface, these stresses being referred to as Marangoni stresses [7]. Investigations by Radoëv et al. [8], Traykov and Ivanov [9], Za-

* Corresponding author.
E-mail address: o.matar@ic.ac.uk (O.K. Matar).

0021-9797/03/$ – see front matter
PII: S0021-9797(02)00033-4

pryanov et al. [10], Sharma and Ruckenstein [11], Li [12], Danov et al. [13], and Valkovska et al. [14], among others, have shown that the presence of surfactants can have a significant effect on the drainage and stability of the continuous phase film and thus on the coalescence of bubbles and drops. In these studies, with the exception of [8] where a constant surfactant concentration was adopted, a *quasi-steady-state* approximation was assumed. Under this approximation, all the variables in the system are implicitly time-dependent through the variation of the local film thickness [13,15]. The local values for the surfactant concentration and the interfacial tension were assumed to deviate only slightly from their equilibrium values and hence were represented by the sums of the corresponding equilibrium values prior to the commencement of the flow and the perturbations to the equilibrium values caused by the flow, expanded to leading order.

More recently, Chesters and Bazhlekov [16] and Yeo et al. [17] considered the dynamic evolution of the surfactant concentration by solving the film evolution equation coupled with the equation governing the interfacial transport of insoluble surfactant. In the latter case, an initially localized *nonuniform* distribution of insoluble surfactant concentration was considered. The nonuniformity in the surfactant concentration thus resulted in the generation of Marangoni stresses, which led to the deformation of the interface and hence the drainage of the film, all of which was taken to occur in a small region far upstream from the dimple rim region (the dimple being formed due to the inversion of the interface from a convex to a concave shape as a result of a balance of the normal stresses). Chesters and Bazhlekov [16], on the other hand, allowed for the interfacial deformation as a result of the axisymmetric approach of the drops to cause a nonuniformity in the surfactant interfacial concentration, which was distributed in a uniform fashion initially onto the then undeformed interface. Thus, in this case, the interfacial concentration gradients arise and evolve from a uniform surfactant concentration distribution due to interfacial deformation occurring during the film drainage process such that the Marangoni effect is driven by the hydrodynamic processes [17].

There are two asymptotic boundary conditions for film drainage: Constant approach force and constant approach velocity [18]. The work of Chesters and Bazhlekov [16] investigates the case of constant force collisions which are characterized by buoyancy-driven collisions. The constant approach velocity boundary condition, on the other hand, is more appropriate for flow-driven collisions where inertial forces are dominant over viscous forces in the draining film, this case being of much relevance in practical liquid–liquid systems. In constant approach velocity collisions, the interaction force increases as the drops approach one another [6]. If the drops fail to coalesce, the force decreases again as the drops separate. Constant approach velocity is usually a good approximation until a significant proportion of the interfacial deformation energy is converted from the kinetic energy available from the collision [19]. At this point, the approach velocity decreases.

This paper focuses on constant approach velocity collisions and highlights the differences in dynamics that arise in this situation from those in the constant force case [16]. We also show that adding even a slight amount of insoluble surfactant results in the immobilization of the interface. Although this has been previously reported both theoretically and experimentally [6,20,21], we have endeavoured to supplement these studies by comparing film drainage profiles between those for a pure system and those for an interface laden with surfactant. In addition, we show the results of a full parametric study of the drainage process, which has identified three different regimes of drainage. The key distinguishing factors between these regimes are the van der Waals interaction force and the velocity of approach.

This paper also considers briefly the mechanism of formation of secondary dispersions. These dispersions (also known as dual dispersions, double dispersions, or multiple dispersions) are dispersions in which the continuous phase is trapped as droplets within the drops of the dispersed phase. The existence of oil droplets enclosed within water drops in pure water-in-oil dispersions has been well-documented in studies such as those by Rodger et al. [22], Quinn and Sigloh [23], and Luhning and Sawistowski [24]. Observations of oil-in-water-in-oil dispersions in systems containing surfactants were reported by Brooks and Richmond [25]. On the other hand, water-in-oil-in-water dispersions have been observed by Luhning and Sawistowski [24], Groeneweg et al. [26], Campbell et al. [27], and Hou and Papadopoulos [28], the latter two investigators working with systems in which surfactants were present. In recent years, it has been postulated that the existence of secondary dispersions plays an important role in phase inversion (the spontaneous interchange of phases whereby the dispersed phase inverts to become the continuous phase and vice versa given a perturbation made to the system properties, energy input or the phase volume holdup) [26,29]. This paper includes a brief section on the estimation of the size of the secondary droplet enclosed into the resultant coalesced drop when two drops collide and the continuous phase film trapped between them drains to its critical rupture thickness as a function of various system parameters.

Conventionally, the coupling between the flow in the film and in the dispersed phase has always been treated by assuming creeping flow or Stokes flow within the drop. This approach has been used by workers such as Klaseboer et al. [6], Chesters and Bazhlekov [16], Yiantsios and Davis [30], Cristini et al. [31], and Bławzdziewicz et al. [32], among others. These studies reported the approach and deformation of viscous drops at constant approach force under the influence of surfactant, with the exception of [6] and [30], where pure systems were assumed. In this paper, however, we consider the feasibility of a simplified approach in which the flow within the drop is described by lubrication theory, a concept first introduced by Li and Liu [33] to

solve a problem related to the one under consideration in this work. A comparison of the results in the present model with that of [6] is encouraging: The close agreement between the predictions indicate that this simplified approach can reproduce the results of the more complex method involving the solution of Stokes flow within the drop phase.

The rest of this paper is organized into the following sections: Section 2 describes the mathematical model to be solved by providing a derivation of the equations together with a list of assumptions made; the relevant scalings and the initial and boundary conditions used are also included. We then discuss the numerical method used to solve the equations derived and briefly validate our model with the results of previous work. A comparison of the model predictions with those obtained assuming Stokes flow within the drop is also included. Section 3 is devoted to an analysis of the results which examines the various effects of the parameters governing the system, such as the viscosity ratio, the surface Péclet number, the drop approach velocity, and the van der Waals interaction force, on the drainage process, as well as the possibility of secondary droplet formation. Finally, the conclusions are provided in Section 4.

2. Mathematical formulation and solution methodology

We consider a system of two initially undeformed spherical drops, each with radius R_i^* $(i = 1, 2)$, approaching each other at a constant approach velocity V^* along the line of their centers in the z-direction, the asterisk denoting dimensional quantities. A schematic representation of the drops as they approach each other and deform is shown in Fig. 1. In a cylindrical coordinate system, the interfaces between the dispersed phases and the draining film are axisymmetric, i.e.,

$$z^* = h_i^*(r^*, t^*), \tag{1}$$

where $h_i^* = \frac{h^*}{2}$ is the film thickness bounded between the plane $z^* = 0$ and the interface of drop i, as shown in Fig. 1, and t^* is the time. It thus follows from axisymmetry that we need only consider the quadrant $r^* \geqslant 0$.

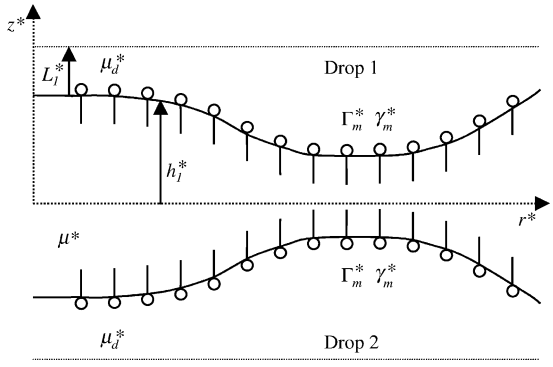

Fig. 1. Schematic representation of the drainage region between two drops.

In addition, the following assumptions, similar to those made in [17], have been adopted in this study to simplify the mathematical model:

1. The film in the region of consideration is sufficiently thin, such that we can impose the following condition:

$$\epsilon \equiv \frac{h_0^*}{R_0^*} \ll 1, \tag{2}$$

where ϵ is a small parameter describing the ratio of the axial to radial length scales, and h_0^* and R_0^* are the initial film thickness at $r^* = 0$ and the initial rim radius, respectively. It is then possible to apply the lubrication approximation [34]. Gravitational forces are also neglected.
2. The dispersed and the continuous phases are incompressible and Newtonian.
3. In the drop, the lubrication approximation also applies such that the velocity and the velocity gradient vanish at a length from the interface, L_i^*, which is the characteristic circulation length of viscous penetration in drop i given by [17,33]

$$L_i^* = \frac{h_0^* R_i^*}{R_0^*}. \tag{3}$$

If L_i^* is assumed to be small compared to the drop radius, R_i^*, then the axial component of the pressure distribution in the drop is negligible compared to its radial component.
4. Since the film is thin in comparison with the region in which the hydrodynamic interaction of the drops occurs, which in turn is small compared to the drop radius (i.e., $h_0^* \ll R_0^* \ll R_i^*$), the consequence of the variation in drop radii on the curvature of the film is negligible. Thus, we can assume symmetry relative to the plane $z^* = 0$ and also write an equivalent radius, R^*, for which the drainage of the film between two drops of equal sizes, R^*, is equal to that between drops of differing sizes, R_1^* and R_2^* [6,35]:

$$\frac{1}{R^*} = \frac{1}{2}\left(\frac{1}{R_1^*} + \frac{1}{R_2^*}\right). \tag{4}$$

5. Since symmetry at the plane $z^* = 0$ is assumed above, it is also possible to assume that the interfacial properties are the same at both interfaces [13,36]: $\gamma_1^* = \gamma_2^* = \gamma^*$, wherein γ_i^* is the interfacial tension at the interface of drop i, which is a function of the interfacial concentration of insoluble surfactant, Γ^*.
6. A dilute monolayer of surfactant with uniform concentration Γ_0^* is placed at the interface initially. The surfactant is assumed to be insoluble in both the dispersed and the continuous phases. The insolubility of the surfactant in the dispersed and the continuous phases is a good approximation for dilute surfactant concentrations where the partition coefficient favors adsorption of the

surfactant at the interface [37]. This is also a good approximation when diffusion of surfactant between the bulk and the interface occurs much faster than the time taken for the film to drain [16]. It is also assumed that steric hindrances and changes in the dilational and shear interfacial viscosities due to the presence of surfactant at the interface do not come into play.

7. We incorporate disjoining pressure effects into the model only by taking into account van der Waals forces. Electric double-layer effects are assumed to be negligible.

2.1. Governing equations

For axisymmetric, incompressible flow, the radial component of the Navier–Stokes equations of motion in the film and in the adjacent dispersed phases can be written as

$$\frac{\partial v_r^*}{\partial t^*} + v_r^*\frac{\partial v_r^*}{\partial r^*} + v_z^*\frac{\partial v_r^*}{\partial z^*} = -\frac{1}{\rho^*}\frac{\partial p^*}{\partial r^*} + \frac{\mu^*}{\rho^*}\left\{\frac{\partial}{\partial r^*}\left[\frac{1}{r^*}\frac{\partial}{\partial r^*}\left(r^* v_r^*\right)\right] + \frac{\partial^2 v_r^*}{\partial z^{*2}}\right\}, \quad (5)$$

and

$$\frac{\partial v_{r_i}^*}{\partial t^*} + v_{r_i}^*\frac{\partial v_{r_i}^*}{\partial r^*} + v_{z_i}^*\frac{\partial v_{r_i}^*}{\partial z^*} = -\frac{1}{\rho_d^*}\frac{\partial p_i^*}{\partial r^*} + \frac{\mu_d^*}{\rho_d^*}\left\{\frac{\partial}{\partial r^*}\left[\frac{1}{r^*}\frac{\partial}{\partial r^*}\left(r^* v_{r_i}^*\right)\right] + \frac{\partial^2 v_{r_i}^*}{\partial z^{*2}}\right\}, \quad (6)$$

respectively. v_r^* and v_z^* are the radial and axial velocities, respectively, and p^* is the pressure; subscript i denotes dispersed phase quantities. In the equations above, μ^* and ρ^* represent the viscosity and the density in the continuous phase, whereas μ_d^* and ρ_d^* denote that in the dispersed phase.

The following set of scalings are adopted to formulate the problem in terms of dimensionless variables:

$$r \equiv \frac{r^*}{R_0^*}; \qquad z \equiv \frac{z^*}{h_0^*}; \qquad h \equiv \frac{h^*}{h_0^*}; \qquad p \equiv \frac{h_0^*}{S^*}p^*;$$
$$t \equiv \frac{\epsilon S^*}{\mu^* R_0^*}t^*; \qquad v_r \equiv \frac{\mu^*}{\epsilon S^*}v_r^*; \qquad \lambda \equiv \frac{\mu_d^*}{\mu^*};$$
$$R_i \equiv \frac{R_i^*}{R_0^*}; \qquad \Gamma \equiv \frac{\Gamma^*}{\Gamma_m^*}; \qquad \gamma \equiv \frac{(\gamma^* - \gamma_m^*)}{S^*}. \quad (7)$$

Here, h is the film thickness and γ_0^* and γ_m^* are the interfacial tensions corresponding to a region of relatively uncontaminated interface and that of the interfacial region saturated with surfactant at concentration Γ_m^*, respectively. We thus define a spreading pressure, S^*, where $S^* = \gamma_0^* - \gamma_m^*$.

On substituting the dimensionless variables in Eq. (7) into the governing equations of motion described in Eqs. (5) and (6), we arrive at

$$Re\left(\frac{\partial v_r}{\partial t} + v_r\frac{\partial v_r}{\partial r} + v_z\frac{\partial v_r}{\partial z}\right) = -\frac{1}{\epsilon}\frac{\partial p}{\partial r} + \epsilon\frac{\partial}{\partial r}\left[\frac{1}{r}\frac{\partial}{\partial r}(r v_r)\right] + \frac{1}{\epsilon}\frac{\partial^2 v_r}{\partial z^2} \quad (8)$$

and

$$Re_d\left(\frac{\partial v_{r_i}}{\partial t} + v_{r_i}\frac{\partial v_{r_i}}{\partial r} + v_{z_i}\frac{\partial v_{r_i}}{\partial z}\right) = -\frac{1}{\epsilon}\frac{\partial p_i}{\partial r} + \epsilon\lambda\frac{\partial}{\partial r}\left[\frac{1}{r}\frac{\partial}{\partial r}(r v_{r_i})\right] + \frac{\lambda}{\epsilon}\frac{\partial^2 v_{r_i}}{\partial z^2}, \quad (9)$$

where Re and Re_d are the Reynolds numbers for the film and the dispersed phase defined by

$$Re = \frac{\rho^*\epsilon S^* h_0^*}{\mu^{*2}}; \qquad Re_d = \frac{\rho_d^*\epsilon S^* h_0^*}{\mu^{*2}}, \quad (10)$$

respectively. From assumption 1, we note that $\epsilon \ll 1$. In this limit, Eqs. (8) and (9) reduce to the usual lubrication equations:

$$\frac{\partial p}{\partial r} = \frac{\partial^2 v_r}{\partial z^2}, \quad (11)$$

for the film and

$$\frac{\partial p_i}{\partial r} = \lambda\frac{\partial^2 v_{r_i}}{\partial z^2}, \quad (12)$$

for the drops.

It should be noted that a different choice of scaling for the film pressure,

$$p \equiv \frac{h_0^*}{\epsilon^2 S^*}p^*, \quad (13)$$

would have reduced the governing equations to

$$\frac{\partial^2 v_r}{\partial z^2} = 0, \quad (14)$$

which would have rendered the radial velocity independent of z to leading order for weak Marangoni stresses. Extensional stresses balance the pressure gradient to next order:

$$\frac{\partial p}{\partial r} = \frac{\partial^2 v_r}{\partial r^2}. \quad (15)$$

However, this case is limited to systems in which the surfactant is present in trace quantities. When Marangoni stresses are considerable at the interfaces to leading order, $S^* \sim O(1)$, and hence the pressure scales as in Eq. (7), resulting in the lubrication approximation in the film described by Eq. (11).

Equation (12) can be integrated with the boundary conditions that specify the velocity and the velocity gradient in the drop, both of which approach zero at a characteristic length $L_i = L_i^*/h_0^*$ (see assumption 3), to give an expression for the dispersed phase radial velocity as follows:

$$v_{r_i} = \frac{[z - (h_i \pm R)]^2}{2\lambda}\frac{\partial p_i}{\partial r}. \quad (16)$$

In Eq. (16), the addition and subtraction signs correspond to $i = 1$ and $i = 2$, respectively.

At the interfaces, we take into account the additional Marangoni stress component that arise due to the interfacial tension gradient. The tangential shear stress balance thus

reads

$$\left.\frac{\partial v_r}{\partial z}\right|_{z=h_1} - \lambda \left.\frac{\partial v_{r_1}}{\partial z}\right|_{z=h_1} = \frac{\partial \gamma}{\partial r}, \tag{17}$$

$$\lambda \left.\frac{\partial v_{r_2}}{\partial z}\right|_{z=h_2} - \left.\frac{\partial v_r}{\partial z}\right|_{z=h_2} = \frac{\partial \gamma}{\partial r}. \tag{18}$$

It should be noted that the term describing the interfacial viscosity, μ_s^*, in the tangential shear stress balance,

$$\mu_s^* \left[\frac{1}{r}\frac{\partial}{\partial r}(r v_{r_{\text{int}}})\right],$$

where $v_{r_{\text{int}}}$ is the radial component of the interfacial velocity, has been omitted from Eqs. (17) and (18) above. This is justifiable since it can be shown that when the scaling laws in Eq. (7) are applied, this term is multiplied by the small parameter ϵ (from assumption 1, we note that $\epsilon \ll 1$).

Substituting Eqs. (17) and (18) into Eq. (16), we can write the drop velocities v_{r_1} and v_{r_2} in terms of the film pressure gradient, $\partial p/\partial r$. At the interfaces, i.e., $z = h_i$,

$$v_{r_{\text{int}}} = \frac{R}{2\lambda}\frac{\partial \gamma}{\partial r} - \frac{hR}{4\lambda}\frac{\partial p}{\partial r}. \tag{19}$$

By taking into account symmetry at the plane $z = 0$, and applying continuity of velocity at both drop interfaces, i.e.,

$$v_r|_{z=h_i} = v_{r_{\text{int}}} \quad (i = 1, 2), \tag{20}$$

we derive the radial film velocity by integration of Eq. (11):

$$v_r = \frac{z^2}{2}\frac{\partial p}{\partial r} - \frac{h}{4\lambda}\left(\frac{\lambda h}{2} + R\right)\frac{\partial p}{\partial r} + \frac{R}{2\lambda}\frac{\partial \gamma}{\partial r}. \tag{21}$$

The kinematic boundary condition is expressed by

$$\frac{\partial h}{\partial t} = -\frac{1}{r}\frac{\partial}{\partial r}(rh\overline{v_r}), \tag{22}$$

where $\overline{v_r}$ is the mean radial film velocity, defined by

$$\overline{v_r} = \frac{1}{h}\int_0^h v_r\, dz. \tag{23}$$

From Eqs. (19), (21), and (22), the film evolution equation can then be derived as follows:

$$\frac{\partial h}{\partial t} = \frac{1}{12r}\frac{\partial}{\partial r}\left(rh^3\frac{\partial p}{\partial r}\right) - \frac{1}{r}\frac{\partial}{\partial r}(rhv_{r_{\text{int}}}). \tag{24}$$

The dimensional normal stress balance across the interface can be written as

$$p^* = \frac{2\gamma^*}{R^*} - \frac{\gamma^*}{2}\left[\frac{1}{r^*}\frac{\partial}{\partial r^*}\left(r^*\frac{\partial h^*}{\partial r^*}\right)\right] + \left(\Phi_\infty^* + \frac{B^*}{h^{*m}}\right), \tag{25}$$

where Φ_∞^* is the van der Waals interaction potential per unit volume of a semi-infinite liquid film in the limit of approaching the liquid–liquid interface, B^* is the Hamaker constant, and m is a parameter. Typically, $B^* \sim 10^{-19}$ erg cm and $m = 4$ for film thicknesses over 400 Å whereas $B^* \sim 10^{-14}$ erg and $m = 3$ for film thicknesses below 120 Å [1,38]. We define the following dimensionless quantities:

$$\Phi_\infty \equiv \frac{h_0^*}{S^*}\Phi_\infty^*; \qquad B \equiv \frac{B^*}{S^* h_0^{*m-1}}. \tag{26}$$

The order of magnitude estimates for all physical constants as well as the typical values for the dimensionless groups used are summarized in Tables 1 and 2, respectively.

Table 1
Typical values for the physical constants used

Physical constant	Typical values
m	3[a,b]
B^*	10^{-21} J[a,b]
γ_m^*	40 dyn/cm
S^*	40 dyn/cm

[a] Applicable for film thicknesses less than 120 Å.
[b] Chen [1]; Chen and Slattery [38].

Table 2
Typical values for the dimensionless groups used

Dimensionless group	Typical values
ϵ	10^{-2}
R	4[a]
h_{00}	1[b]
λ	0.1–100
Pe_s	1–10,000
Γ_0	0.001–0.1
B	10^{-6}–10^{-3}
V	0.1–1.5

[a] Li and Liu [33].
[b] Unless stated otherwise.

Inserting the scalings defined in Eq. (7) into Eq. (25), and utilizing the assumption that $\epsilon \ll 1$ (assumption 1), the dimensionless pressure in the film becomes

$$p = \frac{2}{R}\frac{\epsilon\gamma_m^*}{S^*} - \frac{1}{2}\frac{\epsilon^2\gamma_m^*}{S^*}\left[\frac{1}{r}\frac{\partial}{\partial r}\left(r\frac{\partial h}{\partial r}\right)\right] + \left(\Phi_\infty + \frac{B}{h^m}\right). \tag{27}$$

The surfactant transport equation,

$$\frac{\partial \Gamma^*}{\partial t^*} + \frac{1}{r^*}\frac{\partial}{\partial r^*}\left(r^* v_{r_{\text{int}}}^* \Gamma^*\right) = D_s^*\left[\frac{1}{r^*}\frac{\partial}{\partial r^*}\left(r^*\frac{\partial \Gamma^*}{\partial r^*}\right)\right], \tag{28}$$

in which D_s^* is the surface diffusivity, governs the evolution of the surfactant interfacial concentration. In terms of dimensionless variables,

$$\frac{\partial \Gamma}{\partial t} + \frac{1}{r}\frac{\partial}{\partial r}(r v_{r_{\text{int}}}\Gamma) = \frac{1}{Pe_s}\left[\frac{1}{r}\frac{\partial}{\partial r}\left(r\frac{\partial \Gamma}{\partial r}\right)\right]. \tag{29}$$

In Eq. (29), the surface Péclet number, Pe_s, is defined as

$$Pe_s = \frac{S^* h_0^*}{\mu^* D_s^*}. \tag{30}$$

This dimensionless group describes the ratio of surfactant spreading due to Marangoni stresses to that by surface diffusion. Typically, values for Pe_s between 1 and 10,000 have been used, as listed in Table 2. In the limits of extremely high Péclet numbers, surface diffusion effects become negligible and hence the term on the right-hand side of Eq. (29) vanishes. Nevertheless, we retain this term in these limits as it includes the highest order derivative in the surfactant concentration evolution equation; omission of this term leads to a singular perturbation, giving rise to boundary-layer-like regions in which the concentration will vary rapidly. Inclusion of this term, although as small as some of the other terms neglected in the model (such as the term accounting for the variation of the surfactant concentration due to local changes in the interfacial area, which scales like ϵ^2 under the scaling laws considered), aids the numerics and leads to smoother concentration profiles.

To close the above set of equations, we choose a linear surfactant equation of state, which can be justified for dilute surfactant concentrations:

$$\gamma^* = \gamma_0^* + \left(\frac{\partial \gamma^*}{\partial \Gamma^*}\right)\Gamma^*. \tag{31}$$

Since $\Gamma^* = \Gamma_m^*$ when $\gamma^* = \gamma_m^*$, the dimensionless equation of state reads

$$\gamma = 1 - \Gamma. \tag{32}$$

2.2. Initial and boundary conditions

Initially, the drops are undeformed and thus the film thickness can be approximated by the following parabolic profile

$$h^*(r^*, 0) = h_{00}^* + \frac{{r^*}^2}{R^*}, \tag{33}$$

where h_{00}^* is the initial film thickness at $r^* = 0$. In terms of dimensionless variables, the initial film profile is

$$h(r, 0) = h_{00} + \frac{r^2}{\epsilon R}, \tag{34}$$

where $h_{00} = h_{00}^*/h_0^*$. Surfactant is uniformly distributed on the undeformed interfaces with concentration Γ_0. Thus,

$$\Gamma(r, 0) = \Gamma_0. \tag{35}$$

The boundary conditions for the model are as follows. In the film, symmetry at $r = 0$ requires

$$\left.\frac{\partial h}{\partial r}\right|_{r=0} = 0. \tag{36}$$

Due to symmetry at $r = 0$, we also require $\partial p/\partial r = 0$ [21]. From Eq. (27), we arrive at

$$\left.\frac{\partial^3 h}{\partial r^3}\right|_{r=0} = 0. \tag{37}$$

Far from the drainage region, for sufficiently large r, r_∞, the thinning rate of the film is approximated by the approach velocity of the drops:

$$\left.\frac{\partial h}{\partial t}\right|_{r=r_\infty} = -V; \tag{38}$$

where, in the light of the scaling,

$$V = \frac{V^* \mu^*}{\epsilon^2 S^*}. \tag{39}$$

Far from the drainage region, the excess pressure also tends to zero:

$$p|_{r=r_\infty} = 0. \tag{40}$$

For the surfactant concentration, the boundary conditions are

$$\left.\frac{\partial \Gamma}{\partial r}\right|_{r=0} = 0, \tag{41}$$

and

$$\left.\frac{\partial \Gamma}{\partial r}\right|_{r=r_\infty} = 0. \tag{42}$$

2.3. Method of solution

We solve the two coupled fourth-order nonlinear parabolic partial differential equations that describe the dynamic evolution of the film thickness and the surfactant interfacial concentration, as given by Eqs. (24) and (29), subject to the initial and boundary conditions (34)–(42), numerically using the Method of Lines [39]. The spatial derivatives were discretized using fourth-order centered differences whereas Gear's method was used for the time derivatives [40].

We obtain numerical solutions for the film thickness and the surfactant concentration using the parameter values for Pe_s, λ, B, and V given in Table 2. The simulations were carried out using a uniform grid of 1000 points on a computational spatial domain of up to a maximum length of 14 dimensionless units for times of the order 1000 dimensionless units; convergence was achieved by refining the mesh size of the grid. In addition, we have checked that the solution satisfying the no-flux boundary condition at r_∞ given by Eq. (42) are identical to those obtained with $\Gamma|_{r=r_\infty} = \Gamma_0$, provided that the spatial domain is sufficiently large. In the case of film rupture, the computations were halted when the minimum film thickness was approximately 0.1 due to the difficulty in resolving accurately the increasingly singular spatial derivatives in the rupture region. The rupture times quoted therefore correspond to the time at which the computations were halted.

We validate the numerical scheme against the results of Klaseboer et al. [6] who modeled the surfactant-free film drainage between colliding drops at constant approach velocity for two asymptotic limits: Fully mobile interfaces and fully immobile interfaces. For the fully immobile case, the solution methodologies are the same and hence we used our numerical scheme to solve the dimensionless form of

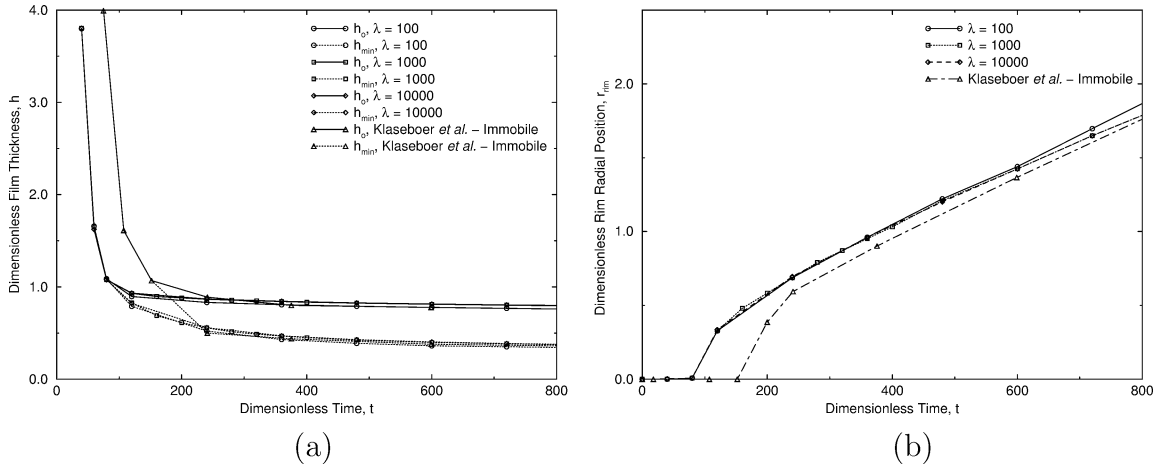

Fig. 2. Comparisons of (a) the evolution of the film thickness at the center, h_0, and at the rim, $h_{\min}$, and (b) the radial rim position $r_{\rm rim}$ for various viscosity ratios with the results of Klaseboer et al. [6] for the fully immobile case generated from the numerical scheme used in this paper and from Fig. 4 found in [6]. The simulation was carried out with the following parameter values: $B = 0$ and $V = 0.5$. In this case, $h_{00} = 17.89$.

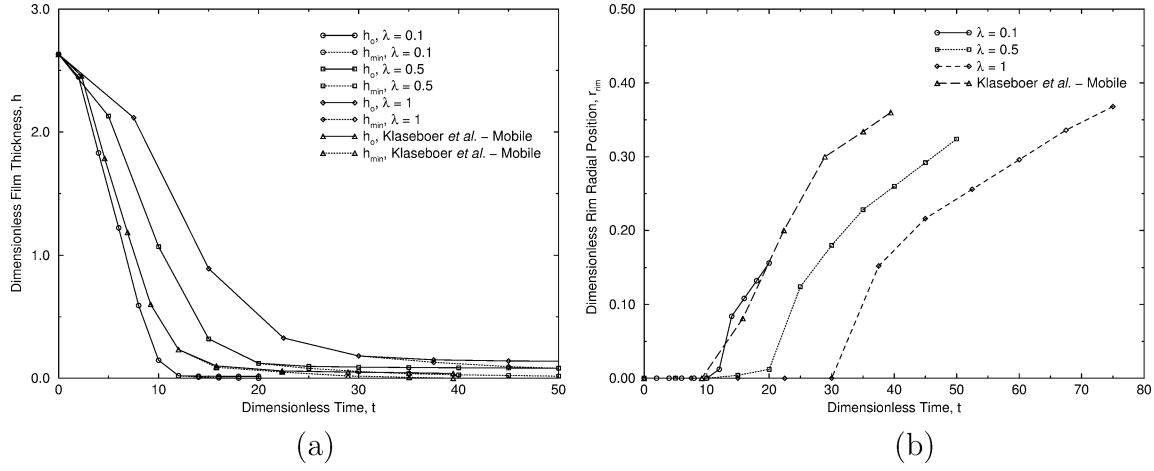

Fig. 3. Comparisons of (a) the evolution of the film thickness at the center, h_0, and at the rim, $h_{\min}$, and (b) the radial rim position, $r_{\rm rim}$, generated from the numerical scheme used in this paper for various viscosity ratios with the results for the fully mobile case found in Fig. 10 of Klaseboer et al. [6]. The simulation was carried out with the following parameter values: $B = 0$ and $V = 0.5$. In this case, $h_{00} = 2.632$.

the governing equations given in [6]. Direct comparisons between the numerical results generated here and those reported in [6] are shown in Figs. 2a and 2b. It can be seen that, within the limit of uncertainties arising from the difficulty in obtaining accurately the numerical results from Fig. 4 given in [6], the agreement is good. Figures 2a and 2b also show that, at large viscosity ratios, the numerical solution for the fully immobile interface limit is recovered.

To test our simplified approach of using lubrication theory to describe the flow within the drops, the predictions of the current model are compared to the results for the fully mobile interface limit of [6], in which the boundary integral method is utilised to solve for Stokes flow in the drops. The results, illustrated in Figs. 3a and 3b, show that as the viscosity ratio is decreased, the fully mobile interface limit is reached. In addition, the film thickness evolution profiles obtained in the present work are also very similar to those found in Fig. 10 of [6]. The close agreement between these results thus inspires confidence in the predictions of our approach and indicates that although it may be possible that interfacial motion drives a Stokes flow within the drop, the effect of this flow appears to be confined to the contact region between the film and the drop, namely, the characteristic circulation length of viscous penetration.

3. Discussion of results

We begin the discussion of our results in Section 3.1 by describing the effect of adding insoluble surfactant to a surfactant-free system. In the sections following 3.1, a brief parametric study is undertaken where various dimensionless groups and parameters are examined in sequence: Section 3.2 is devoted to investigating the effects of the surface Péclet number, Pe_s, and the viscosity ratio, λ, on film

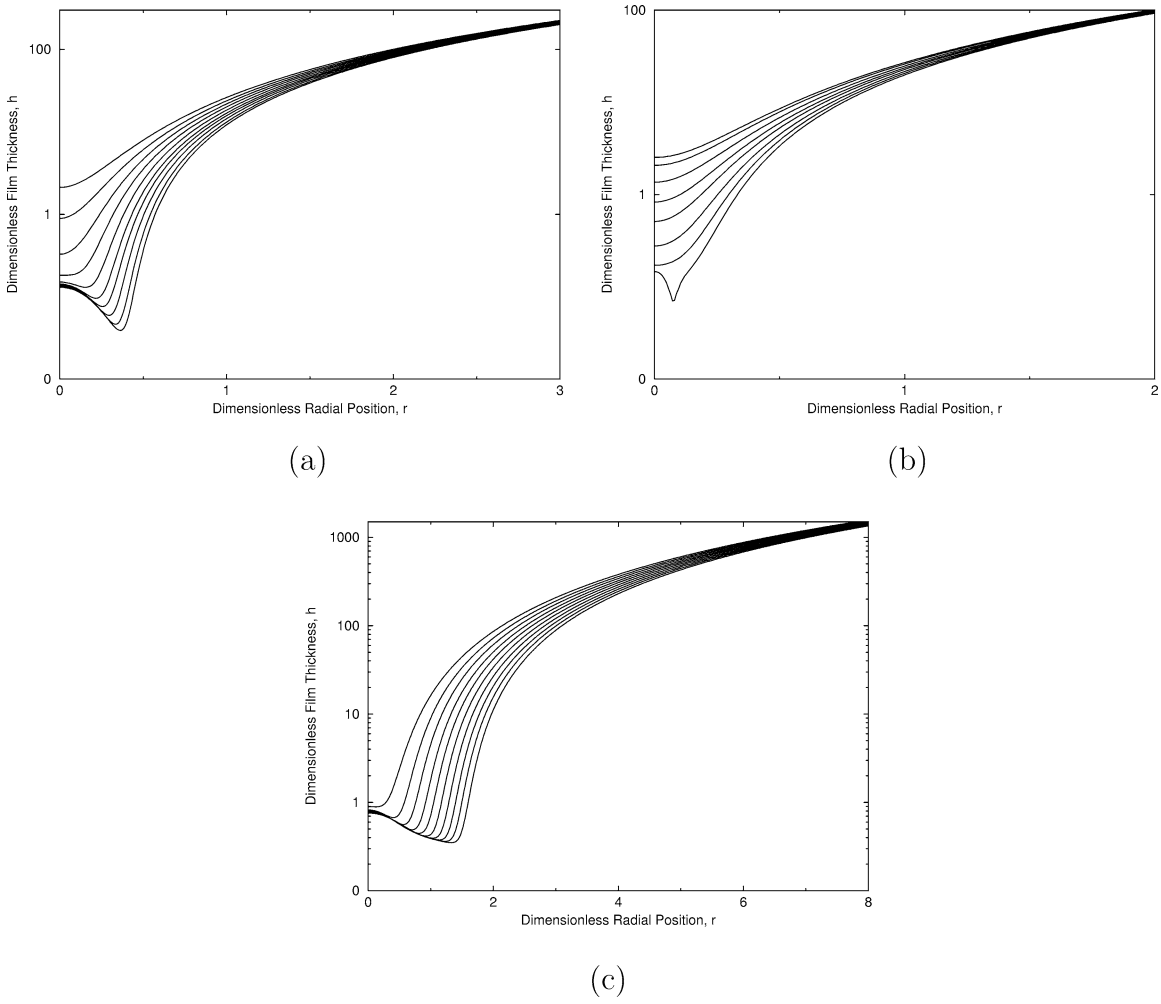

Fig. 4. Film thickness profiles for (a) surfactant-free system without van der Waals interactions up to $t = 75$ in equal time steps; (b) surfactant-free system with van der Waals interactions up to $t = 31.25$ in equal time steps ($B = 10^{-5}$); (c) surfactant-laden system with van der Waals interactions up to $t = 600$ in equal time steps ($Pe_s = 10{,}000$, $\Gamma_0 = 0.1$, and $B = 10^{-5}$). The rest of the parameter values are $\lambda = 1$ and $V = 0.5$. Here, $h_{00} = 2.632$ to match the conditions given in [6].

drainage. The influence of the approach velocity and the van der Waals interaction forces on drainage and rupture are considered in Section 3.3. Finally, in Section 3.4, we briefly discuss the possibility of forming secondary droplets.

3.1. Interface immobilization

Figure 4a illustrates a typical film evolution profile for a surfactant-free system in the absence of van der Waals forces for $\lambda = 1$ and $V = 0.5$. It can be seen that the film initially thins and deforms. This is due to an insufficient pressure in the drop to overcome the normal viscous stress associated with the pressure in the film [14]. If the drop pressure is still insufficient to overcome the pressure in the flattened film, the interface inverts from a convex to a concave shape such that the interfacial curvature goes from zero to negative to balance the normal stresses and thus a "dimple" is formed.

The profile for the same system under the influence of van der Waals attractive forces is shown in Fig. 4b. It can be seen that the film quickly ruptures even under the influence of a weak interaction force. When surfactant is added to this system, the film thins much more slowly, thus prolonging rupture to later times, or preventing it altogether. In the case chosen, the film, which had ruptured at $t = 31.25$ in the absence of surfactant, has still not undergone rupture when surfactant was added to the system even at $t = 600$, as seen in Fig. 4c.

A typical spatio-temporal evolution profile of initially uniform surfactant interfacial concentration is illustrated in Fig. 5a for $\lambda = 1$, $Pe_s = 10{,}000$, $\Gamma_0 = 0.1$, $B = 10^{-5}$, and $V = 0.1$. As the film drains due to the approach of the drops, the deformation of the film near the center of the drops results in a depletion in the surfactant concentration. This depletion continues until concentration gradients are large enough to cause Marangoni stresses to refill the surfactant-depleted region, with the exception of the rim region of the dimple, shown in Fig. 5b. As the rim of the dimple spreads out, the well in the concentration profile also shifts outward. At very low film thicknesses where the van der Waals forces become significant and the film tends to rupture, both

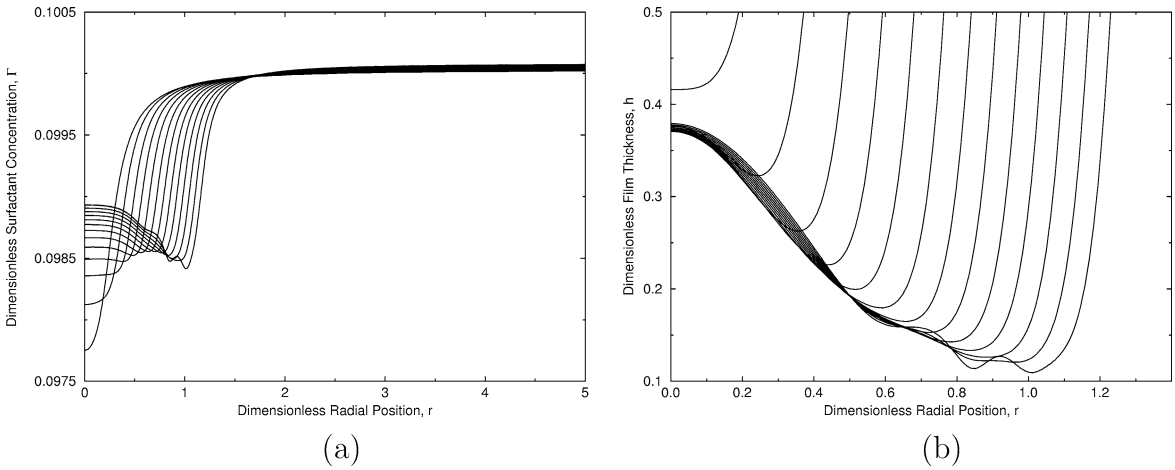

Fig. 5. Typical surfactant concentration (a) and film thickness (b) evolution profile for 13 equal time steps up to $t = 1473$. Parameter values are $\lambda = 1$, $Pe_s = 10{,}000$, $\Gamma_0 = 0.1$, $B = 10^{-5}$, and $V = 0.1$.

continuous phase liquid and surfactant are expelled from this rim region, resulting in a sharp depletion in the surfactant concentration. This, in turn, causes large interfacial tension gradients which attempt to replenish the rim region with surfactant, dragging along with it the continuous phase liquid. These competing effects give rise to a low amplitude wavelike structure at the rim region in both h and Γ, as seen in Fig. 5b. The amplitude of this wave is accentuated as the magnitude of the van der Waals interaction force is increased, the wave being absent when B was set to zero. The structure of the wave remained unchanged upon mesh refinement, suggesting that its origins are physical rather than numerical.

The wavelike profile observed here is probably related to the non-uniformities observed in the photographs of the film during its thinning in the work of Manev et al. [41]. These periodic interfacial inhomogeneities were observed at very small film thicknesses, close to the critical rupture thickness. Later work by Radoev et al. [42] and Sharma and Ruckenstein [43] also confirmed that these inhomogeneities are significant near the unstable region, the growth of these finite amplitude hydrodynamic interfacial waves occuring within about 50 Å of the critical rupture thickness. The appearance of our interfacial waves in the later stages of film thickness close to the point of film rupture seems to be consistent with these observations. In addition, the amplitude and the wavelength of the interfacial wave observed in Fig. 5b also seem to be of the same order of magnitude with that observed by Radoev et al. [42] where amplitudes of the order 100 Å and wavelengths of the order 10^{-3} cm were observed. Sharma and Ruckenstein [43] have suggested that it is the "pumping" action on the fluid in the film generated by these hydrodynamic interfacial waves moving outward toward the film periphery that enhances the rate of film drainage in the region of the critical film thickness. Consequently, the instant at which the film ruptures and the critical thickness at which this occurs depends on these periodic waves.

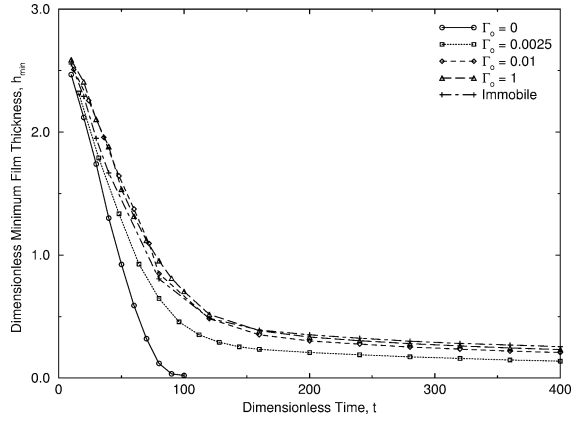

Fig. 6. Comparison of the minimum film thickness with time for the case of the surfactant-free system, for surfactant-free system with immobile interfaces, and for surfactant-laden systems with $\Gamma_0 = 0.0025$, 0.01, and 1. The remaining parameter values are $\lambda = 1$, $B = 0$, and $V = 0.05$. Where applicable, $Pe_s = 10{,}000$. For the fully immobile case, $h_{00} = 17.89$ to match conditions given in [6].

Figure 6 shows the rate of thinning for various systems: Surfactant-free system, surfactant-free immobile interfaces, and systems containing surfactant at different initial concentrations. The parameters used are $\lambda = 1$, $B = 0$, and $V = 0.05$. For the surfactant-free immobile interface case, relevant for systems in which the dispersed to continuous phase viscosity ratio is high, there is no interfacial motion (i.e., $v_{r_{\text{int}}} = 0$) and hence the plug flow contribution is zero. For this limiting case, the film evolution equation given in Eq. (24) reduces to a parabolic velocity profile (Poiseuille flow) wherein the flow is only driven by the radial pressure gradient of the film:

$$\frac{\partial h}{\partial t} = \frac{1}{12r}\frac{\partial}{\partial r}\left(rh^3\frac{\partial p}{\partial r}\right). \tag{43}$$

It can be seen that the rate of film drainage decreases rapidly with the addition of surfactant such that, at some saturation value, $\Gamma_0 = 0.01$, the interface is rendered fully immobile.

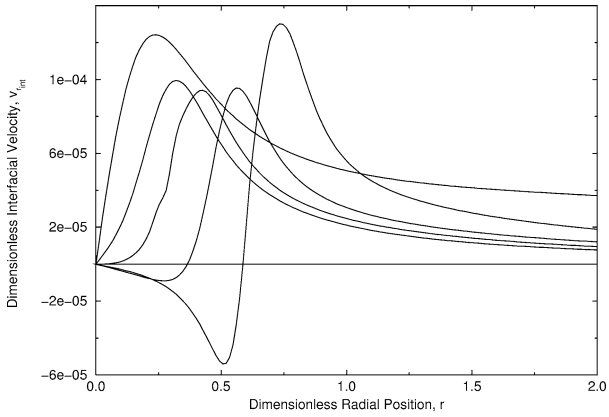

Fig. 7. Profiles of the interfacial velocity, $v_{r_{\mathrm{int}}}$, for times $t = 30.0$, 72.0, 108.0, 180.0, and 300.0 for $\lambda = 1$, $Pe_s = 1000$, $\Gamma_0 = 0.1$, $B = 10^{-4}$, and $V = 0.25$.

This result confirms the observations of several investigators [6,20,21] who have reported that only a small amount of surfactant concentration is sufficient to immobilize the interface since the interfacial tension gradients that arise due to the presence of surfactant are oriented in such a way that they oppose any mobility at the interface.

The drainage dynamics exhibited in this case of constant approach velocity are significantly different from those for collisions under constant approach force studied by Chesters and Bazhlekov [16]. In their case, the film thins and flattens, and subsequently forms a dimple. However, because of the convection of surfactant away from the dimple region, the Marangoni effect refills the region at the film periphery with surfactant, dragging along with it the interface, resulting in the disappearance of the dimple. The dimple then regrows spontaneously soon after due to the hydrodynamic pressure in the film overcoming the negative interfacial velocity caused by the motion of surfactant back into the dimple region. While the mechanism for the transport of surfactant back into the dimple region by the Marangoni stresses is the same in both the constant approach velocity and the constant approach force cases, it should be noted that the concentration gradients that arise in the latter case are much larger than that found in our results. Careful examination of the surfactant concentration profiles in [16] shows that the surfactant is almost completely depleted whereas Fig. 5a shows that, in the constant approach velocity case, the relative proportion of surfactant depleted is only minute. As a result, there are insufficient Marangoni stresses to overcome the positive velocity gradient outward due to the hydrodynamic pressure in the film. Since the interfacial velocity is never negative at any point in time during the early stages of film drainage as shown in Fig. 7, the dimple does not refill, even though there is a refilling of surfactant into the dimple region. The Marangoni stresses only succeed in retarding the film drainage but never in causing film thickening. In fact, only negative interfacial velocities are observed in the rupture region (see Fig. 7), which explains why the film is replenished in this region to form the wavy film reported earlier in Fig. 5b.

A plausible explanation for the difference in the decrease in surfactant concentration during the initial stages of film drainage for the asymptotic cases of constant approach velocity and constant approach force are the magnitudes of the interaction forces under which the initial drainage occurs. In the constant approach force case, the initially high approach velocity decreases continually to zero to maintain a constant force of approach between the drops. Since the approach velocity is initially very high and the approach force is at its constant value in the initial stages of film drainage, there is a large force to cause significant deformation to the film and hence to deplete the surfactant almost completely at the dimple region. Subsequently, the approach velocity decreases and the drainage slows down. The large surfactant concentration gradients produced initially are now in place to cause a negative interfacial velocity, resulting in the refilling of the dimple region. On the other hand, for the constant approach velocity case, the approach force is small to begin with but increases as the drops approach [6]. As a result, the deformation is not substantial enough to deplete the surfactant concentration in the dimple region by very significant amounts. However, as the approach force increases very rapidly shortly after, the drainage takes place very quickly while the surfactant concentration gradients, which have arisen in the initial stages of drainage, are insufficient to cause a negative interface velocity to refill the dimple.

3.2. Effect of surface Péclet number and viscosity ratio

Surface Péclet numbers, Pe_s, in the range between 1 and 10,000 were studied. At low Pe_s, the dominant mechanism of surfactant transport is surface diffusion whereas Marangoni convection dominates the transport of surfactant in the limit of high Pe_s, i.e., $Pe_s \gg O(1)$. To examine the full spectrum of diffusive to convective spreading, we consider Pe_s in the range between 1 and 10,000. The plots of minimum film thickness against time for various Pe_s in Fig. 8 show that film drainage occurs rapidly for low values of Pe_s. As Pe_s is increased, the thinning of the film is slowed down and the dimpling of the film also begins to occur for the case of $Pe_s = 1000$, evidenced by the slight flattening of the minimum film thickness profile as seen in Fig. 8. In Section 3.1 it was shown that the Marangoni effect, which occurs when the concentration gradient becomes sufficiently large, acts to refill the surfactant-depleted zone where the thinning of the film occurs. The interfacial velocity is therefore retarded by the Marangoni stresses, slowing down film thinning. Nevertheless, as was also mentioned in Section 3.1, the concentration gradients are insufficient to cause negative interfacial velocities such that the liquid film is returned to the dimple region. On the other hand, at low Pe_s, surfactant transport is dominated by diffusion rather than Marangoni stresses, with negligible retardation effects on film drainage.

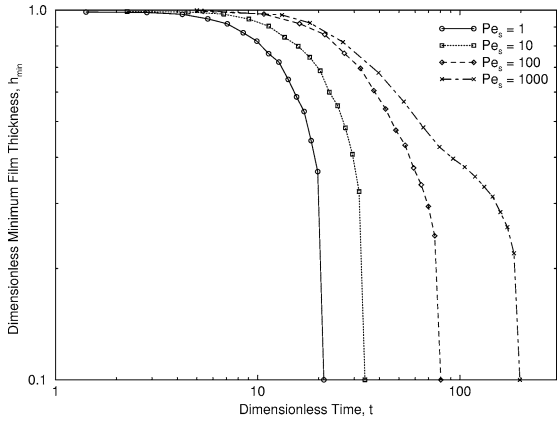

Fig. 8. Variation of the minimum film thickness with time as a function of the surface Péclet number, Pe_s. The other parameters are $\lambda = 1$, $\Gamma_0 = 0.1$, $B = 10^{-4}$, and $V = 0.1$.

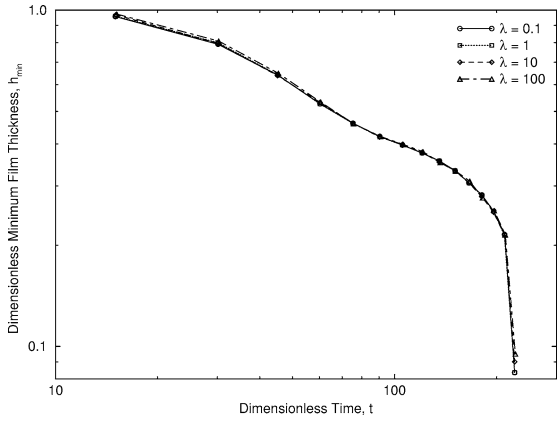

Fig. 9. Minimum film thickness as a function of time for various viscosity ratios. The remaining parameters are held constant at $Pe_s = 10{,}000$, $\Gamma_0 = 0.1$, $B = 10^{-4}$, and $V = 0.1$.

The effect of the viscosity ratios was also examined, the results of which are shown in Fig. 9. To isolate the effects of λ, the study was carried out by keeping all other parameters constant ($Pe_s = 10{,}000$, $\Gamma_0 = 0.1$, $B = 10^{-4}$, and $V = 0.1$). For systems in which the surface Péclet number is sufficiently large such that Marangoni convection is the dominant mechanism for surfactant transport, the plots indicate that the viscosity ratio plays a negligible role in the drainage of the film, an observation which is consistent with the experimental results of Klaseboer et al. [6]. This is as expected because the interfaces are immobilized by the presence of surfactant for large Pe_s systems [6,16]. In other words, for large Pe_s, the effect of the flow in the adjacent drop phase is negligible and therefore the film drainage is independent of the dispersed phase viscosity and hence the viscosity ratio.

3.3. Effect of approach velocity and van der Waals interaction on film rupture

The evolution profiles of the film thickness and the surfactant concentration for three approach velocities, $V = 0.1$, 0.5, and 1.5 are shown in Figs. 10–12. The remainder of the system parameters are $\lambda = 1$, $Pe_s = 10{,}000$, $\Gamma_0 = 0.1$, and $B = 10^{-3}$. When the drops collide at low approach velocities, film thinning occurs rapidly and rupture occurs in the nose region. Dimpling does not occur because, at low approach velocities, the hydrodynamic force is insufficient to deform the film. As the drops collide with greater approach velocities, it can be seen that dimpling begins to occur, therefore retarding the thinning of the film. The film dimples in the case of greater approach velocities because the pressure in the flattened film exceeds that in the drop. For the normal stresses to balance, there is therefore an inversion of the interface curvature. Rupture then occurs at the rim, the radial position of the rim at the rupture point increasing with approach velocity, in agreement with [6].

The effect of varying the magnitude of van der Waals interactions on the drainage dynamics was also studied; electric double-layer effects are not considered. Fig. 13, which depicts the minimum film thickness for various values of the dimensionless Hamaker constant B using $\lambda = 1$, $Pe_s = 10{,}000$, $\Gamma_0 = 0.1$, and $V = 0.1$, shows that the time taken for the film to rupture decreases with increasing B. For $B = 10^{-6}$, the van der Waals force is extremely weak and hence the film does not rupture. Rather, the dimple becomes wider as the dimple rim extends outward with the flow in the film. In this case, little thinning occurs. With large values of B, the critical rupture thickness is large because strong van der Waals forces are able to cause the film to rupture even for films with relatively large thicknesses. Under these circumstances, the van der Waals attraction prevails over the hydrodynamic resistance of the film pressure. The film thus thins more rapidly in the center at the axis of symmetry than in the downstream regions. This leads to a protrusion at the center, resulting in film rupture in that region before any significant deformation or dimpling can occur. In other words, a so-called "pimple" [14] forms, leading to a mode of rupture known as *nose rupture* [30]. An example of this is shown in Fig. 10a wherein the low approach velocity does not provide sufficient hydrodynamic resistance to overcome the negative disjoining pressure arising from the van der Waals force. On the other hand, small values of the Hamaker constant require the film to drain to smaller length scales at which the weak van der Waals forces becomes significant. For extremely small values of the Hamaker constant, the film is immobilized at thicknesses larger than the length scale at which the van der Waals force becomes significant. As a result, the film does not rupture but becomes progressively flat. Between these limits of Hamaker constants, the film thins due to the hydrodynamic forces, leading to the formation of the dimple, and subsequently ruptures along the curvature at the rim of the dimple. This rupture mode is referred to in the literature as *rim rupture* [30].

In summary, three different regimes of film drainage are identified: Pimple formation leading to nose rupture, dimple formation leading to rim rupture, and interface immobiliza-

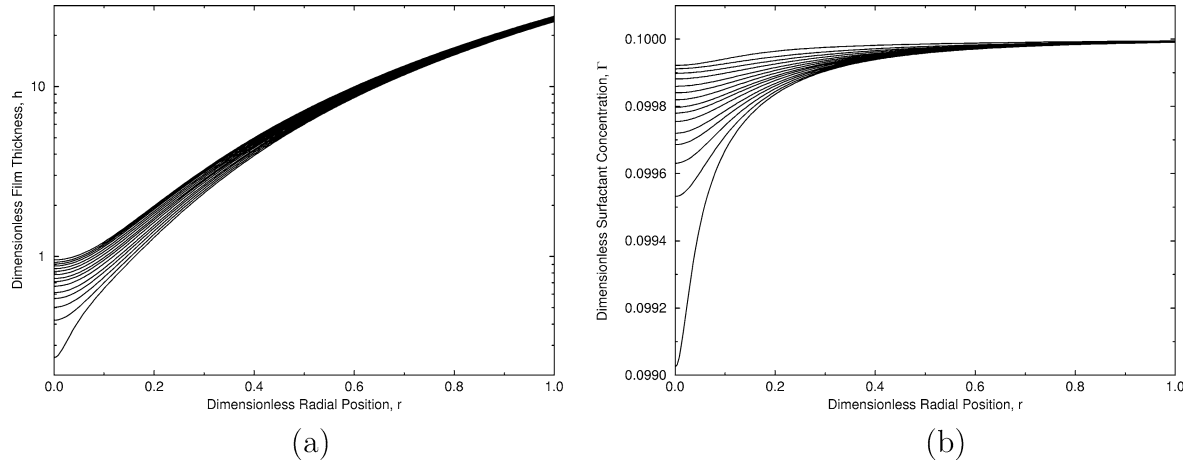

Fig. 10. Film thickness (a) and surfactant concentration (b) profiles for 15 equal time steps up to $t = 29.9$ for $\lambda = 1$, $Pe_s = 10{,}000$, $\Gamma_0 = 0.1$, $B = 10^{-3}$, and $V = 0.1$.

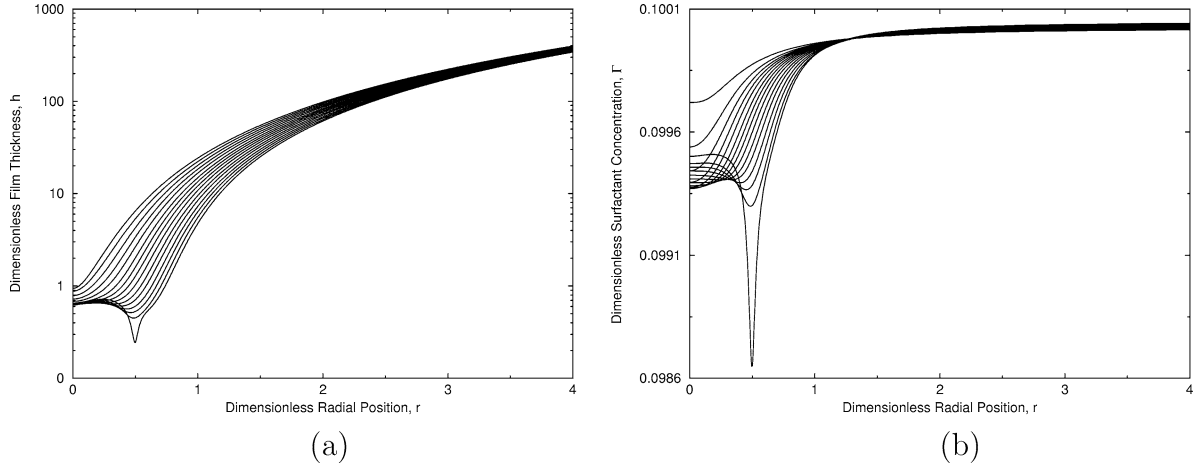

Fig. 11. Film thickness (a) and surfactant concentration (b) profiles for 15 equal time steps up to $t = 62.2$ for $\lambda = 1$, $Pe_s = 10{,}000$, $\Gamma_0 = 0.1$, $B = 10^{-3}$, and $V = 0.5$.

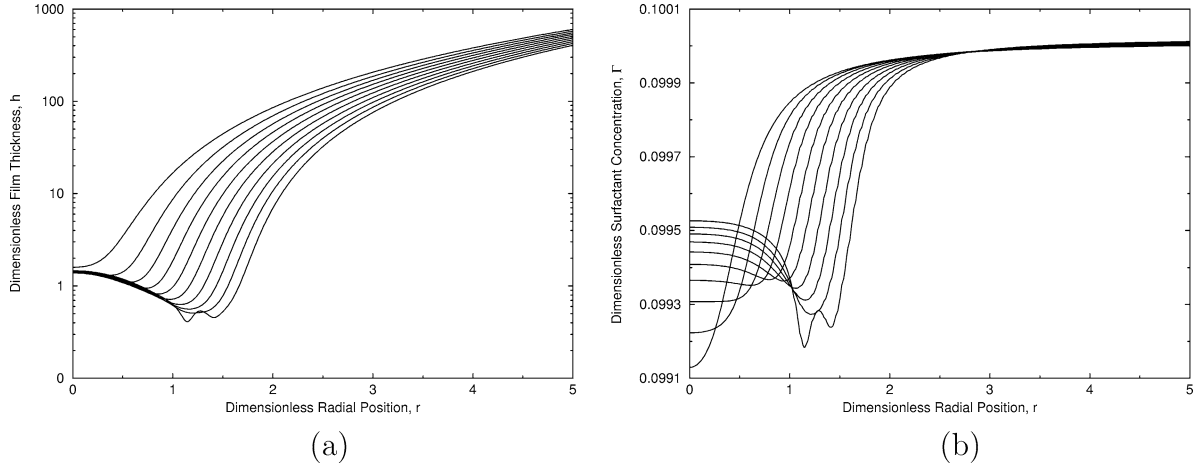

Fig. 12. Film thickness (a) and surfactant concentration (b) profiles for 10 equal time steps up to $t = 267.3$ for $\lambda = 1$, $Pe_s = 10{,}000$, $\Gamma_0 = 0.1$, $B = 10^{-3}$, and $V = 1.5$.

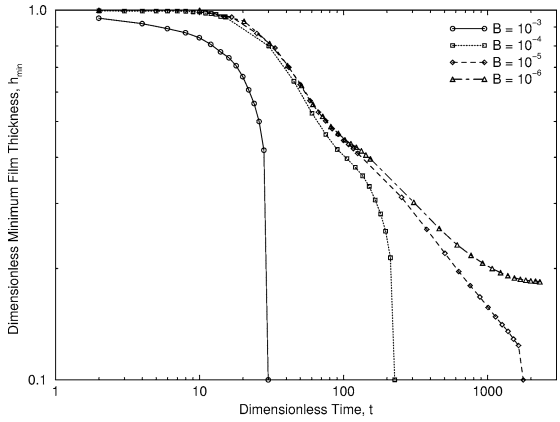

Fig. 13. Evolution of the minimum film thickness with time for various dimensionless Hamaker constants, B. Other parameters are $\lambda = 1$, $Pe_s = 10{,}000$, $\Gamma_0 = 0.1$, and $V = 0.1$.

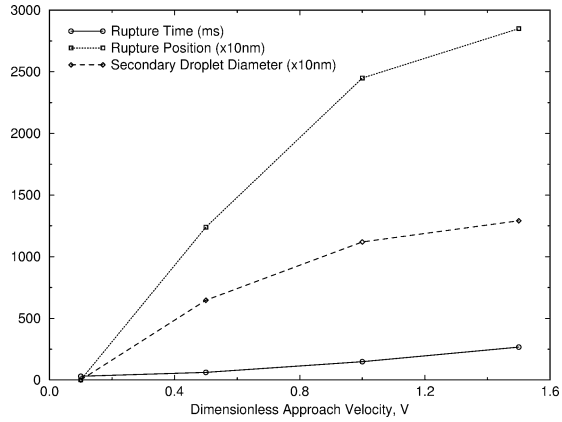

Fig. 14. Rupture time, radial rupture position, and the size of the secondary droplet enclosed as a function of the approach velocity, V. The other parameter values are $\lambda = 1$, $Pe_s = 10{,}000$, $\Gamma_0 = 0.1$, and $B = 10^{-3}$.

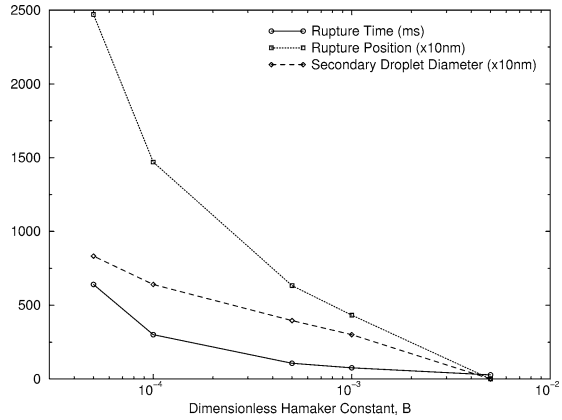

Fig. 15. Rupture time, radial rupture position, and the size of the secondary droplet enclosed as a function of the dimensionless Hamaker constant, B. The remaining parameter values are $\lambda = 1$, $Pe_s = 1000$, $\Gamma_0 = 0.1$, and $V = 0.25$.

tion prior to the action of negative disjoining pressure forces, resulting in a nearly flat film. The resulting type of regime depends largely on the relative magnitudes of the approach velocity and the negative contribution to the disjoining pressure provided by the van der Waals interactions. Low approach velocities and strong van der Waals interactions lead to the formation of a pimple and rupture in the nose region, whereas high approach velocities and weak van der Waals interactions lead to dimple formation, which either ruptures or flattens out to form an almost parallel film.

3.4. The formation of secondary droplets

When rim rupture occurs, a small amount of the continuous phase is encapsulated into the coalesced drop to form a secondary droplet or a droplet within a drop [26,30]. The condition for secondary droplet formation arising from binary collisions is therefore for rupture to occur at the rim. This is in agreement with the work of Groeneweg et al. [26], who suggested that the entrapment of a secondary droplet occurs when the inertial collision between two drops, is sufficiently intense that the intervening continuous phase film becomes adequately flattened. It thus follows from our discussion in the section above that the collision intensity would depend on the velocity of approach of the drops; the greater the approach velocity, the more intense the collision. In addition, we suggest from our results above that the magnitude of the interaction forces also affects the probability of secondary droplet formation. Weak van der Waals interactions lead to a flattened film, which does not proceed toward rupture during the contact time of the drops. Strong van der Waals interactions, on the other hand, lead to nose rupture and hence no secondary drop formation.

Figures 14 and 15 show the rupture time, the radial position of the rupture point and the diameter of the secondary droplet encapsulated as a function of the drop approach velocity and the dimensionless Hamaker constant, respectively. The dimensionless volume of the secondary droplet, V_{sd}, is calculated from the following integral:

$$V_{\mathrm{sd}} = 2\pi \int_0^{r_m} rh\,dr, \tag{44}$$

where r_m is the dimensionless rim radius at which point rupture occurs. The diameter of the secondary droplet can then be calculated from this volume, assuming it to be spherical in shape. The sizes of the secondary droplet calculated are based on an initial film thickness of 1 μm and an initial drop radius of 100 μm. It is worthy of mention that the size of the calculated secondary droplets are of the order of those estimated in [26]: For drops of the size 300–400 μm, Groeneweg et al. [26] estimated the enclosed droplets to be 8 μm. The figures also indicate that the size of the secondary droplet encapsulated into the coalesced drop increases as the magnitude of the approach velocity increases but is inversely proportional to the magnitude of the van der Waals interaction. More generally, the diameter of the secondary droplet formed would depend on the system

parameters governing the selection of the rupture modes, as discussed in the previous section.

The trend of increasing droplet sizes with increasing magnitude of the approach velocity in Fig. 14, however, will not continue since there will be rupture times which will exceed the drop contact time. Levich [44] assumes the average contact time, t_c^*, to be proportional to the characteristic period of velocity fluctuation for an eddy of size $(d_1^* + d_2^*)$, where d_1^* and d_2^* are the diameters of the colliding drops and thus

$$t_c^* \sim \frac{(d_1^* + d_2^*)^{2/3}}{\epsilon_d^{*1/3}}, \tag{45}$$

ϵ_d^* being the energy dissipation per unit mass ($\epsilon_d^* \sim N^{*3} D_I^{*2}$), where N^* is the agitation speed and D_I^* is the impeller diameter. Based on experimental conditions given in [45], we estimate from Eq. (45) that contact times are of the order 0.1 s. Therefore, from Fig. 14 it can be seen that there will be a cut-off point for the rupture time and thus for the approach velocity beyond which no secondary droplet will be formed.

4. Conclusions

In this paper, we have presented an investigation of the drainage dynamics of the intervening continuous phase film trapped between two drops coated with an initially uniform concentration of insoluble surfactant approaching one another at constant velocity. The objective of this work is generally threefold: (1) To briefly consider the feasibility of using a simplified approach of applying the lubrication approximation within the drops; (2) to demonstrate that interfacial immobilization can occur in the presence of even a small concentration of surfactant; (3) to highlight the differences in dynamics between this constant approach velocity case and that of the constant force case [16].

These objectives are met numerically by solving the fully coupled system of partial differential equations governing interfacial deformation and surfactant transport, closed with appropriate initial and boundary conditions and a linear surfactant equation of state. The close agreement between the results of our study with those of Klaseboer et al. [6], who adopted the assumption of Stokes flow within the dispersed phase, inspires confidence in our simplified approach of assuming lubrication theory to describe the flow within the drops. It also indicates that the effect of the flow arising within the drop is restricted to the contact region between the film and the drop, which we have termed as the characteristic circulation length of viscous penetration.

Our results indicate that hydrodynamic forces resulting from drop collisions give rise to surfactant-depleted regions locally near the flow origin. This, in turn, leads to the formation of surfactant concentration gradients which act to retard the drainage of the film, resulting in immobilization. In the presence of negative disjoining pressures, there is a possibility that film rupture may be prolonged and possibly prevented by adding surfactant to the interface; in certain cases, low amplitude interfacial waves, not unlike those previously reported in the literature [11,41–43], were also observed at the rim. We note that, above a critical value for the initial surfactant concentration, the drainage profile tends to follow that of a system with fully immobile interfaces, this concentration being of order 0.01 of the saturation value. While these are observations which have been reported in the literature [6,20,21], we have developed a dynamically evolving model which describes well these phenomena and allows for the comparison of the film evolution profiles for surfactant-free, fully immobile, and surfactant-laden systems.

We have also shown that the degree of surfactant depletion, and hence the magnitude of Marangoni stresses, in the constant velocity case are substantially smaller than those in the constant force [16] case. Consequently, the dimple-refilling and subsequent redimpling phenomena observed in the latter case are not present in the former case studied here.

Our parametric study revealed that the effect of the viscosity ratio on film drainage is largely insignificant when the film is immobilized since the effect of the flow in the drop phase is negligible. Our results also show that the effects of surfactant are rendered essentially insignificant for low surface Péclet numbers, leading to rapid drainage and rupture. This is as expected since diffusive surfactant transport is overwhelmed by hydrodynamic and van der Waals forces.

The role of approach velocities and van der Waals interactions on film drainage and rupture were also examined; three regimes of film drainage and rupture were identified. At low drop approach velocities and when the negative disjoining pressure is strong, the film protrudes at the drop center, forming a pimple, leading to nose rupture. In contrast, a dimple forms which flattens out into an almost parallel film when the approach velocity is high and when negative disjoining pressure effects are weak. In this case, film rupture is averted. Between these two limiting cases for moderate approach velocities and van der Waals interactions, a dimple forms and rim rupture occurs.

These regimes have a bearing on the possibility of the continuous phase film being encapsulated into the coalesced drop as a secondary droplet. The conditions for secondary droplet inclusion are therefore moderate approach velocities and van der Waals attraction such that a dimple forms and rupture occurs at the rim; the size of the secondary droplet increases with increasing film flattening, that is, at larger approach velocities and weaker van der Waals interactions.

References

[1] J.D. Chen, J. Colloid Interface Sci. 107 (1985) 209.
[2] G.E. Charles, S.G. Mason, J. Colloid Sci. 15 (1960) 236.
[3] A.F. Jones, S.D.R. Wilson, J. Fluid Mech. 87 (1978) 263.
[4] P.D. Howell, J. Eng. Math. 35 (1999) 271.

[5] D. Li, J. Colloid Interface Sci. 163 (1994) 108.
[6] E. Klaseboer, J.Ph. Chevaillier, C. Gourdon, O. Masbernat, J. Colloid Interface Sci. 229 (2000) 274.
[7] D.A. Edwards, H. Brenner, D.T. Wasan, Interfacial Transport Processes and Rheology, Butterworth–Heinemann, London, 1991.
[8] B.P. Radoëv, D.S. Dimitrov, I.B. Ivanov, Colloid Polym. Sci. 252 (1974) 50.
[9] T.T. Traykov, I.B. Ivanov, Int. J. Multiphase Flow 3 (1977) 471.
[10] Z. Zapryanov, A.K. Malhotra, N. Aderangi, D.T. Wasan, Int. J. Multiphase Flow 9 (1983) 105.
[11] A. Sharma, E. Ruckenstein, Colloid Polym. Sci. 266 (1988) 60.
[12] D. Li, J. Colloid Interface Sci. 181 (1996) 34.
[13] K.D. Danov, D.S. Valkovska, I.B. Ivanov, J. Colloid Interface Sci. 211 (1999) 291.
[14] D.S. Valkovska, K.D. Danov, I.B. Ivanov, Colloid Surf. A 175 (2000) 179.
[15] I.B. Ivanov, D.S. Dimitrov, P. Somasundaran, R.K. Jain, Chem. Eng. Sci. 40 (1985) 137.
[16] A.K. Chesters, I.B. Bazhlekov, J. Colloid Interface Sci. 230 (2000) 229.
[17] L.Y. Yeo, O.K. Matar, E.S. Perez de Ortiz, G.F. Hewitt, J. Colloid Interface Sci. 241 (2001) 233.
[18] A.K. Chesters, Chem. Eng. Res. Des., Trans. IChemE A 69 (1991) 259.
[19] S. Abid, A.K. Chesters, Int. J. Multiphase Flow 20 (1994) 613.
[20] R.S. Allan, G.E. Charles, S.G. Mason, J. Colloid Sci. 16 (1961) 150.
[21] C.Y. Lin, J.C. Slattery, AIChE J. 28 (1982) 147.
[22] W.A. Rodger, V.G. Trice Jr., J.H. Rushton, Chem. Eng. Prog. 52 (1956) 515.
[23] J.A. Quinn, D.B. Sigloh, Can. J. Chem. Eng. 41 (1963) 15.
[24] R.W. Luhning, H. Sawistowski, in: J.G. Gregory, B. Evans, P.C. Weston (Eds.), Proceedings of the International Solvent Extraction Conference, Vol. 2, Society of Chemical Industry, London, 1971, p. 873.
[25] B.W. Brooks, H.N. Richmond, Colloid Surf. 58 (1991) 131.
[26] F. Groeneweg, W.G.M. Agterof, P. Jaeger, J.J.M. Janssen, J.A. Wieringa, J.K. Klahn, Chem. Eng. Res. Des. A 76 (1998) 55.
[27] I. Campbell, I. Norton, W. Morley, Neth. Milk Dairy J. 50 (1996) 167.
[28] W. Hou, K.D. Papadopoulos, Chem. Eng. Sci. 51 (1996) 5043.
[29] L.Y. Yeo, O.K. Matar, E.S. Perez de Ortiz, G.F. Hewitt, Multiphase Sci. Tech. 12 (2000) 51.
[30] S.G. Yiantsios, R.H. Davis, J. Colloid Interface Sci. 144 (1991) 412.
[31] V. Cristini, J. Bławzdziewicz, M. Loewenberg, J. Fluid Mech. 366 (1998) 259.
[32] J. Bławzdziewicz, E. Wajnryb, M. Loewenberg, J. Fluid Mech. 395 (1999) 29.
[33] D. Li, S. Liu, Langmuir 12 (1996) 5216.
[34] R.H. Davis, J.A. Schonberg, J.M. Rallison, Phys. Fluids A 1 (1989) 77.
[35] S.A.K. Jeelani, S. Hartland, J. Colloid Interface Sci. 206 (1998) 83.
[36] C.Y. Lin, J.C. Slattery, AIChE J. 28 (1982) 786.
[37] W.J. Milliken, H.A. Stone, L.G. Leal, Phys. Fluids A 5 (1993) 69.
[38] J.D. Chen, J.C. Slattery, AIChE J. 28 (1982) 955.
[39] W.E. Schiesser, The Numerical Method of Lines, Academic Press, San Diego, 1991.
[40] O.K. Matar, S.M. Troian, Phys. Fluids A 11 (1999) 3232.
[41] E. Manev, A. Scheludko, D. Exerowa, Colloid Polym. Sci. 252 (1974) 586.
[42] B.P. Radoev, A.D. Scheludko, E.D. Manev, J. Colloid Interface Sci. 95 (1983) 254.
[43] A. Sharma, E. Ruckenstein, J. Colloid Interface Sci. 119 (1987) 14.
[44] V.G. Levich, Physicochemical Hydrodynamics, Prentice–Hall, Englewood Cliffs, NJ, 1962.
[45] C.A. Coulaloglou, Chem. Eng. Sci. 32 (1977) 1289.